Additive Manufacturing 36 (2020) 101469

Contents lists available at ScienceDirect

Additive Manufacturing

journal homepage: www.elsevier.com/locate/addma

Injection printing: additive molding via shell material extrusion and filling

David O. Kazmer*, Austin Colon

Department of Plastics Engineering, University of Massachusetts Lowell, USA

ARTICLE INFO

Keywords:
Injection molding
Material extrusion
Dimensionality
Instrumentation

ABSTRACT

Material extrusion is a popular process for both prototyping and digital manufacturing, yet it is lacking in terms of part strength, feature resolution, and production rate relative to alternative processes. Injection printing addresses these issues by combining material extrusion of the outer surfaces of the part at fine resolution with injection molding of larger interior cavities at high flow rates. Injection printing thus aims to utilize the full melting capacity of material extrusion printers to mitigate the curse of dimensionality that plagues additive manufacturing. Simple governing models for flow in the formed cavities as well as the stress and deflection of the shell walls are presented. To validate the performance of injection printing relative to material extrusion, impact specimens and tensile bars were printed of acrylonitrile butadiene styrene (ABS). The tensile and impact results of the samples were compared, and image analysis was performed on the post-test samples. It was found that injection printing increased print speeds by an average factor of 3.2 relative to conventional material extrusion using the same linear print velocities. With respect to properties, the stiffness, strength, and strain to failure of injection printed tensile bars (in-plane) were respectively increased by 21 %, 47 %, and 35 % compared to material extrusion. Properties of impact specimen and vertically printed tensile bars also showed promising gains albeit with constraints related to the printer's melting capacity. Even still, injection printing is shown as a broadly applicable and readily accessible process for increasing part strength and production rate while enabling improved feature resolution without greatly extended print times.

1. Introduction

Material extrusion, also referred to as fused filament fabrication (FFF) and fused deposition modeling (FDM), is an additive manufacturing technique that deposits roads of molten polymer that solidify into a desired shape. Material extrusion enables the creation of complex designs without tooling that are difficult to produce or otherwise unattainable via traditional manufacturing. Despite the benefits and widespread use of material extrusion, dominating constraints in application of material extrusion may include limited part strength, high degree of anisotropy, poor print resolution, inadequate surface finish, lack of repeatability, uncontrolled shrinkage and warpage, limited process observability and quality assurance, low production rates, very poor energy efficiency, and others.

Some of these deficiencies can be remedied by scaling the material extrusion process to smaller road dimensions so that resolution and surface finish can be improved; Turner and Gold [1] provide a review focusing on the relationship between process and product design parameters and the dimensional and surface properties of finished parts. However, use of smaller roads falls prey to the "curse of dimensionality" [2] wherein the printing in three dimensions causes the printing time to scale with the cube of the resolution relative to the part size. As shown in Fig. 1(a), the roads printed with width W and height H must traverse at velocity V to deposit the part volume. As the road width and height are decreased to improve the resolution and surface roughness, the print times increase dramatically. Since the print head must traverse all coordinates in the X, Y, and Z directions, the dimensionality of the process is 3 such that print time scales with the cube of the resolution.

Other processes such as polyjet [3], powder bed [4], and continuous liquid interface production (CLIP [5],) processes reduce dimensionality to improve print speeds while also delivering fine resolutions. As shown in Fig. 1(b), for example, the polyjet and powder bed fusion printers employ a long print head to parallel print a 1200 dpi (21 μm) resolution line across the Y direction while traversing in the X direction before building in the Z direction; the resulting build dimensionality is 2. As another example, the CLIP process of Fig. 1(c) uses digital light processing with an oxygen and ultraviolet (UV) permeable window to project and process an entire XY layer at once; the resulting build dimensionality is 1. By reducing the dimensionality, these processes can be designed to favorably trade-off the printing resolution and speed.

This article describes and validates an injection printing process as

* Corresponding author at: Department of Plastics Engineering, 1 University Avenue, University of Massachusetts Lowell, Lowell, Massachusetts, 01854, USA.
E-mail address: David_Kazmer@uml.edu (D.O. Kazmer).

https://doi.org/10.1016/j.addma.2020.101469
Received 13 January 2020; Received in revised form 29 May 2020; Accepted 16 July 2020
Available online 20 July 2020
2214-8604/

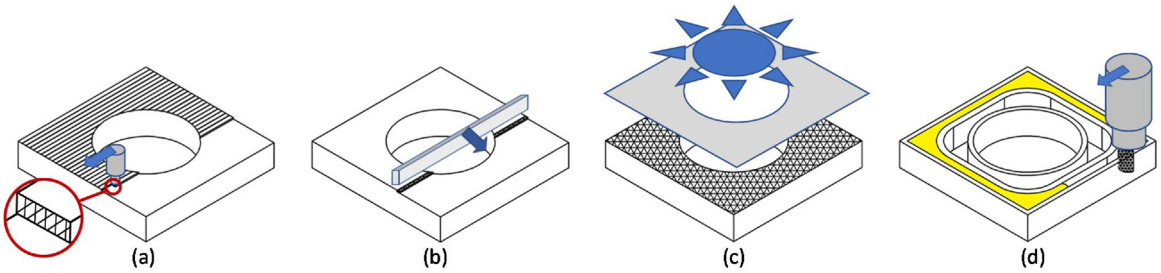

Fig. 1. Additive manufacturing of a simple shape with the hatched area representing the active area of various processes for (a) material extrusion with dimensionality N = 3, (b) polyjet and binderjet processes with N = 2, (c) CLIP process with N = 1, and (d) described injection printing process with N approaching 2.

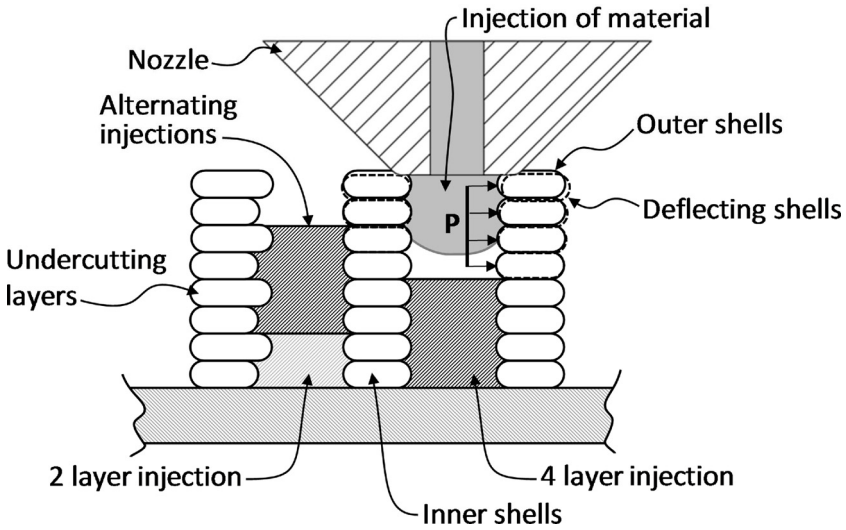

Fig. 2. Section of an injection printing process; material injected into a cavity formed by inner and outer shells develops pressure that stresses and deflects the shells.

depicted in Fig. 1(d) such as with a cross-section shown in Fig. 2. The underlying concept is that multiple roads can be deposited by material extrusion to construct a shell having detailed features and surfaces as well as multiple interior cavities. The interior cavities can then be filled as a bulk process akin to injection molding at much higher volumetric flow rates. Depending on the part geometry, interior shell walls can be used to decompose the width into multiple cavities that can be individually filled. To improve anisotropic properties and impact strength, the depth and shape of the cavities can also be controlled by the pre-processing of the geometry so that the cavity can cross a varying number of shell layers. Fig. 2, for example, shows the injection printing of a part with the cavities offset in the vertical direction to form a checkboard pattern. If desired, the roads forming the shell layers can also be printed with varying widths as shown in the left outer shell. The varying road width allow the formation of undercuts inside the cavity while increasing surface area for bonding with the injected material.

Some related material extrusion processes have been developed primarily to improve print strength. Belter and Dollar [6] describe a method for “fill compositing” additively manufactured parts by material extrusion. They specifically describe carefully placing voids in the printed parts and filling them with high-strength resins (e.g. epoxy) to improve the overall part strength and stiffness by up to 45 % and 25 %, respectively. The described injection printing method differs significantly. Fill compositing provides the second resin after the 3D printed shell is made and removed from the 3D printer. By comparison, injection printing iteratively prints the shell and fills the cavity within a continuous, intertwined process of shell printing and injection to flexibly and quickly print complex geometries with improved properties.

A more closely related work is the “Z-Pinning” approach developed by Duty et al. [7]. In “Z-Pinning”, material is deposited across multiple layers within the volume of the part and was shown to increase the tensile strength and toughness in the z-direction by more than a factor of 3.5 for some materials and processes. However, the injection printing differs with respect to the shape and volume of the cavities formed and injected. Specifically, Z-Pinning (as its name implies) is directed to depositing material through a primarily vertical interstitial matrix to form interlocking structures to improve the part strength. By comparison, injection printing forms relatively large and deep cavities that are filled at much higher volumetric flow rates. In this manner, injection printing is a hybrid process of injeciton molding and material extrusion in which the additively manufactured part is made using its printed shell as its own injection mold. As a result, injection printing enables significant improvements in both deposition rates and material isotropy.

The concept of injection printing is also useful in terms of modeling the efficiency gains afforded by process and machine design in view of the theoretical limits related to curse of dimensionality. The underlying theory pertaining to efficiency and cavity sizing are next presented. Afterwards, the injection printing methods and validation are described, showing increases in print speeds by a factor of 4 on stock printers while also increasing part strength. The discussion will detail how further increases in print speeds are possible by increasing the melting capacity of the hot ends and increasing the nozzle’s contact surface area while also controlling part properties with melt pressure control.

2. Theory

Injection printing significantly increases print speed by allowing large volumes of material to be injected into the printed shell with relatively little nozzle movement. Many material extrusion applications use a hot end and heated nozzle to liquify a solid filament driven by a

feed gear attached to a rotary motor. In such applications, the maximum flow rate for injection can be limited by the heat transfer from the hot end to the colder filament. At high speeds, the filament may not have adequate residence time in the nozzle to attain temperatures sufficient for injection.

The underlying theory is that the power, p, required to liquify the filament is equal to the product of the volumetric flow rate, Q, the density, ρ, the specific heat, C, and the temperature rise ΔT between the filament's desired melt temperature T_2 and the colder filament T_1, such that:

$$p = Q\rho C(T_2 - T_1) \quad (1)$$

Approximate values for acrylonitrile butadiene styrene (ABS) plastic are ρ equal to 1 g/mL, C equal to 2 J/K, T_2 of 230 °C, and T_1 of 100 °C. A typical maximum flow rate for stock printers is around 10 mm^3/s = 0.01 mL/s, such that the required heating power is 3.6 W. While the heater power is known and is often 20 W for consumer printers, much of this power is transmitted from the heated nozzle to the environment and adjoining machine elements; thermal contact resistance between the filament and the hot end as well as the low thermal conductivity of the filament also limit the energy transfer from the heater to the filament [8]. As such, just increasing the heating power does not necessarily greatly increase the heating capacity of the hot end.

Experimental characterization suggests that typical stock printers (e.g. Prusa i3 MK3, Lulzbot Taz6, Creality, Qidi Xpro) are capable of a heating power of around 5 W, corresponding to a volumetric flow rate of 12.5 mL/s for the previously described ABS. How does this relate to injection printing? Well, a typical road that is 0.5 mm wide and 0.1 mm high has a cross sectional area of 0.05 mm^2, such that a volumetric flow rate of 12.5 mL/s would require printing at velocities of 250 mm per second or 15,000 mm per minute. These speeds are far beyond the typical print speeds of 40 or 50 mm/s, which means that stock printers have a lot of available, unused melting capacity.

The injection printing method allows much higher material flow rates by injecting larger volumes into a relatively large cavity without requiring significant traversing velocities. The target volumetric flow rate, Q, can be used to directly compute the minimum cavity dimensions required to utilize the full capacity of the 3D printer. For example, consider a printing application with Q equal to 12.5 mL/s and a traversing print speed, v, of 20 mm/s. Then, the cross-sectional area, A, of the cavity to fully utilize the printer is $A = Q/v$, which equals 0.625 mm^2. As such, a cavity that is 1 mm wide and 0.625 mm high would fully utilize the melting capacity of the printer. Larger cavities can, of course, be produced. For example, a cavity with a width of 2 mm and a depth of 1.25 mm would have a cross-section area of 2.5 mm^2, and so would fully utilize the melting capacity at a velocity, $v = Q/A$, which equals 5 mm/s. While the traversal velocity seems slow, the extruding capability of the 3D printer is being fully utilized. By comparison, the typical printer may deposit a road that is 0.5 mm wide and 0.1 mm high at a speed of 50 mm/s. This process corresponds to a volumetric flow rate of 2.5 mL/s, a full factor of 5 lower than the injection printing method printing at 12.5 mL/s on the same printer. As later described, increases of a factor of more than 4 have been achieved. The speed increase is not just due to the greater volumetric flow rate afforded by the injection printing method, but also due to less repositioning of the nozzle required for printing complex fill patterns composed of many smaller roads and in-fill patterns.

Given that injection printing can greatly increase the volumetric flow rate by filling relatively large cavities, it is desirable to increase the heating capacity of the printer since, at high volumetric flow rates, the filament may flow through the nozzle too quickly to allow adequate heat transfer for the filament temperature to attain the desired melt temperature. At lower temperatures, the viscosity and flow resistance increase so as to make the material difficult to force through the nozzle given the available force or torque driving the filament. At this point, the feed gear will tend to slip along the filament and the filament will temporarily remain stationary until it is sufficiently hot to flow through the nozzle. The stalling of the filament can be detected by a number of ways including (i) the use of a filament position sensor such as described by Coogan [9], (ii) by an audible noise such as a clicking sound emitted by the toothed gear slipping over the filament, or (iii) by the appearance of divots in the deposited roads, which were sometimes observed in our validation trials when attempting to inject material at higher flow rates above 20 mm^3/s. The reason the divots appear is that the nozzle continues to traverse while the filament has temporarily stalled. As such, the appearance of these divots is an indicator that insufficient heat is being transferred to the filament and a drop in the output flow rate has occurred. Interestingly, the behavior at high flow rates is often oscillatory but repeatable with a divot appearing when the filament is too viscous to maintain a high flow rate through the nozzle. The lower flow rate allows the filament to melt in the nozzle and maintain the desired flow rate for a short while until the melt temperature drops and the material again becomes too viscous at which time a new divot appears and the cycle repeats.

Rate limits in material extrusion have been formally investigated [10] with findings that limits on the traction force exerted on the filament and conduction heat transfer to the filament core are dominating constraints. The melting behaviors in hot ends and nozzles is an active area of research [8,11,12], and several approaches are being investigated. One approach is to use a plasticating screw that heats and melts the polymer along a screw channel that provides a melting length much greater than the nozzles used in 3D printing. While such screws are used in big area additive manufacturing [13], it is also possible to increase the effective heating of the filament through nozzle design for an existing 3D printer. Some of the underlying theory is previously investigated with respect to capillary rheometry [14]. Increasing the nozzle length increases the residence time of the filament in the nozzle and so allows greater heating power. However, increasing the nozzle length will also tend to increase the pressure drop. Accordingly, slightly increasing the nozzle outlet diameter, or tapering from a larger diameter to the desired outlet diameter, or stepping with tapers from one or more larger diameters to the desired outlet diameters are preferable ways to increase the heat transfer, volumetric flow rate, and hence printing speed. Increasing the nozzle temperature setpoint, T_2, will also tend to improve the achievable volumetric flow rates through a nozzle. While the foregoing theory suggests a hard limit to the volumetric flow rate, experimentation has shown that it is possible to print at higher volumetric flow rates (e.g. 20 rather than 12.5 mL/s) even when the melt temperatures are not equilibrated. More recently, Go and Hart developed a "FastFFF" process [15] that uses a nut-feed extruder and laser-heated polymer liquefier to respectively achieve high extrusion force and rapid filament heating shown capable of a volumetric build rate of 35 mL/s, approximately seven times greater than commercial material extrusion systems, with the printhead itself capable of a maximum extrusion rate of the of 78 mL/s.

With respect to choosing the cavity size, there are separate benefits for having large and small cavities. Smaller cavities afford lower residence times, so the printed shells will tend to be produced with greater frequency and so have slightly higher surface temperatures that promote diffusion and bonding with themselves and the injected material [16]. Larger cavities afford greater cavity length and widths, both being beneficial for different reasons. Larger cavity widths avoid the need for printing multiple side-by-side cavities with internal shell walls that take require more print time to produce. Larger cavity heights allow the injected material to traverse multiple layers of the printed shell and so produce parts that are stronger in the vertical (Z) direction. While smaller cavities do provide higher surface temperatures for the substrate, larger cavities have not displayed issues with diffusion and bonding. The reason is that larger cavities also afford significant latent heat in the greater mass of the injected material such that the injected material can readily heat and bond with the surrounding shell surfaces.

The size of the cavity is primarily chosen based on flow, structural,

and thermal considerations according to the underlying physics, many of which are readily modeled according to mold design guidelines [17]. The flow of the injected material will tend to enter the cavity in a radial fill pattern, first forming a spherical shape as it leaves the nozzle and then transitioning to a cylindrical or strip shape as constrained by the nearby cavity surfaces. Accordingly, the pressure required to fill the cavity with a Newtonian fluid is the product of the flow rate, Q, and viscosity, η, divided by the flow resistance, R. The flow resistance for a Newtonian fluid in a rectangular cavity is:

$$R = 12L/WH^3 \tag{2}$$

where L is the flow length, W is the cavity width, and H is the cavity thickness. For example, consider the filling of a 2 mm long rectangular cavity with a width and height both equal to 1 mm. If the viscosity is 1000 Pa s and the flow rate is 10 mL/s, then the pressure required to fill the cavity is equal to 240 kPa or 35 psi. This amount of pressure is very small relative to the achievable supply pressures of $5-10$ MPa that can be achieved by material extrusion processes as previously observed with an in-line melt pressure sensor [9]. While this example assumes a Newtonian and isothermal flow, the results provide a useful order of magnitude estimate useful for design and processing purposes. More accurate analysis can be readily performed by analytical and numerical methods. The main point here is that both theory and practice prove that cavities with larger flow lengths and smaller cavity widths and heights can be readily filled with injected material in situ, even when the material is much more viscous than 1000 Pa s, for example. Such flow analysis can be performed as part of the process for planning the formation of the shell walls and injecting the material into the cavities.

Now consider the analysis of the flow and deformation in the cross-section of Fig. 2. As later described, this example corresponds to the production of an impact specimen that is 127 mm long, 3.2 mm wide, and 12.7 mm high. To produce this impact specimen, suppose that the roads are 0.5 mm wide as deposited with a nozzle having an orifice of 0.4 mm and a lateral surface that is 0.9 mm in diameter. To produce a part having a width of 3.18 mm, it is expedient to print two outer and one inner shell walls such as shown in Fig. 2. Then, the two cavities formed between the interior shell wall and each of the two outer walls is approximately 0.85 mm. The structure can be produced by depositing the first two layers of shells, then traversing and filling the length of the left side of the impact specimen to the fill the left cavity. Two additional layers of shells are then printed, after which the right cavity that is four layers deep is filled. The alternating pattern of printing two layers of shells followed by filling a cavity four layers deep is then repeated to form a checkboard patterned cross section. The offset filling of the cavities improves the robustness of the part by allowing the adjoining column of the material to transfer the load across the part should a section of the part contain a defect or break during end-use.

Fig. 2 also demonstrates the use of slight compression of the shell to form a seal with the nozzle during injection of the material into the cavity. The amount of compression is quite small; the figure depicts one quarter of the deposited road height of the shell. The compression provides two benefits. First, the compression allows the injection of material into a cavity that is actually wider than the outer diameter of the nozzle; some of the later validation work employed cavities that were 1.09 mm wide while the outer diameter of the nozzle was 0.9 mm. Second, the compression assists in forming a seal for retaining the injected material within the volume of the cavity within the shell. The compression results in vertical displacement of the unfilled portions of the shell such as indicated by the dashed rounded rectangles. In pre-processing, less compression is provided when injecting into the first few cavities since the relatively low vertical height of the part provides sufficient stiffness for making good seals with less compression.

Considering the structural requirements, the primary design and processing constraints are related to the strength and deflection of the shell wall upon application of internal pressure from the filling of the cavity by injection. As shown in Fig. 2, the injection of material will result in a pressure P indicated by the parallel set of arrows. If the applied pressure results in a shear stress greater than the bond strength of the layers, then the layers may rupture allowing the injected material to escape the shell. Some simple mechanics can be modeled to provide useful estimates and guidelines for pre-processing. The lateral force, F, on the side wall of the cavity is equal to the product of the cavity height, H_C, road length, L, and pressure, P:

$$F = H_C LP \tag{3}$$

This results in a shear stress, τ, at the bottom of the side wall (just above the previously filled cavity) equal to F divided by the product of the road width, W, and road length, L:

$$\tau = H_C LP/LW = P(H_C/W) \tag{4}$$

Accordingly, the shear stress, τ, may be estimated directly as the pressure, P, times the ratio of the cavity height, H_C, to the road width, W. For example, suppose that P is 5 MPa with H_C equal to 0.8 mm and W equal to 0.5 mm such as shown in Fig. 2. Then, the resulting shear stress is equal to 8 MPa. This analysis and later validation indicates that rupture of the shell wall is not a significant limiting constraint since applied pressures are typically far less than 5 MPa and bond strengths are often greater than 8 MPa [16]. The stress analysis is admittedly approximate but sufficiently accurate for pre-processing given a stress constraint on the maximum allowable shear stress. It is straightforward in pre-processing to manage the shear stress by reducing the cavity height, increasing the road and shell width, or printing two, or more, adjacent roads to form thicker shell walls.

The other structural issue is deflection of the shell walls during injection of the material into the cavities. Midway down the length of a long channel, in a worst case scenario, the walls of the shell forming the cavity essentially act as a semi-infinite cantilever beam under a pressure load. The situation is also depicted in Fig. 2 via the dashed rounded rectangles relative to the original road positions. The lateral outward deflection, δ, at the top road can be estimated as approximately:

$$\delta = 4PH_C^4/3EW^3 \tag{5}$$

where E is the modulus of the material comprising the shell wall. The modulus will vary with the material composition and temperature during processing, but is typically one, or more, orders of magnitude greater than the cavity pressure P. Continuing with the prior example of Fig. 2, let E equal 1000 MPa, H_C equal 0.8 mm, and W equal to 0.5 mm. Then the lateral deflection, δ, for a melt pressure of 240 kPa is around 0.001 mm. The amount is measurable but readily managed in practice. Such outward deflections of the shell wall are not typically problematic, and in fact can be beneficial insomuch as they compensate for volumetric shrinkage of the material injected into the cavity as it cools.

The cooling time of the shell also needs to be considered when planning the shell and cavity layouts. In processing of some of the test specimens later shown, for example, rupture of the side wall with escape of the material outside the shell has been seen in cases where the printing was too fast, and the shell walls were not solidified. The heat transfer can be readily modeled by transient heat conduction analysis in one, two, or three dimensions [18]. A useful first order cooling estimate, derived from the analytical solution of the heat equation for typical polymeric materials and processing conditions [17], is that the cooling time, t_c, is approximately equal to the two times the squared apparent thickness (H_A, measured in mm) of the deposited or injected material:

$$t_c = 2\ [\mathrm{s/mm^2}]H_A^2 \tag{6}$$

Here, the apparent thickness is defined as the approximate distance required for heat conduction to cool the hotter deposited material to a heat sink below the solidification temperature. For the example of printing a road for the shell wall of Fig. 2, the apparent thickness would be equal to the road height of 0.2 mm such that the approximate cooling time is 0.08 s. This cooling time is a short compared to the

typical printing time for a given layer. For the material injected into the cavity, the apparent thickness is equal to the cavity width plus some portion of the adjoining shell walls should they also be at an elevated temperature. For the example of Fig. 2, the apparent thickness for cooling is estimated to be around 1.5 mm, which corresponds to a cooling time of 4.5 s. In validation, glossy finishes on the top and outer walls of the printed parts have been observed indicating longer cooling times with relaxation and smoothing of the cavity and outer walls. Such glossy finishes may be highly desirable in application not only for aesthetic purposes but also for structural performance since they are indicative of re-melting of the surrounding area, which produces improved bond strengths and surface finishes. Also, in validation, material deposition rates can be so fast that the added heat exceeds the rate cooling. For example, at the onset of the research, a test impact specimen was made having a length of 25 mm instead of 127 mm with all other conditions the same. The shorter length of the part and more frequent layer deposition increased the rate of heat input per layer relative to the amount of cooling. As such, the part was successfully produced but exhibited slight creep during production such that the height dropped to 12.4 mm from 12.7 mm and the thickness increased to 3.4 mm from 3.2 mm. The entirety of the part was also highly glossy rather than a matte finish. As with the filling and structural considerations, cooling should also be considered in planning of the shells and cavities. If the heat input undesirably exceeds the achievable rate of cooling, issues may be resolved by forced convective cooling, slowing the material deposition and injection rates, or producing multiple parts in parallel to allow the layers and cavities more time to cool.

3. Material and methods

Three part geometries, shown in Fig. 3, were produced for process validation and testing. At left is an impact specimen 127 mm in length, 3.2 mm in width, and 12.7 mm in height. At middle is a horizontal tensile specimen printed within its primary length direction printed parallel to the build plate. Its overall length is 127 mm with a thickness of 3.2 mm. The clamping ends are 17.7 mm wide but neck down via a 50 mm radius to a gage section that is 50.8 mm long and 12.7 mm wide. The right-most specimen of Fig. 3 is a vertical test specimen that was successfully and reliably printed with its primary length normal to the build plate. This vertical tensile specimen has the same geometry as the previously described horizontal tensile specimen. To ensure build plate adhesion and stability, a rectangular raft with triangular connecting struts were designed and printed. This support was subsequently twisted off without adverse effects found during tensile testing.

All process validation was performed with a single spool of Acrylonitrile Butadiene Styrene (HATCHBOX ABS 3D Printer Filament, colored black, Pomona, California USA) having a diameter of 1.75 mm and a dimensional accuracy +/- 0.03 mm. Printing temperatures were set according to material manufacturing guidelines (hot end and nozzle temperature of 230 °C and a build plate temperature of 100 °C) and maintained across all processing trials. The printer was a stock Qidi XPro (Ruian, Zhejiang Province of China) that was unmodified with a nozzle orifice of 0.4 mm. The pre-processing for the reference material extrusion was performed in Ultimaker Cura version 3.2 (Utrecht, Netherlands) using print settings as subsequently described for each test geometry. The injection printing processes were written in g-code using algorithms developed by the first author in MathWorks Matlab (Cambridge, Massachusetts USA).

Table 1
Production and performance statistics for impact specimens.

	Material Extrusion	Injection Printing
Build plate temperature	100 °C	100 °C
Nozzle temperature	230 °C	230 °C
Road/shell width	0.5 mm	0.5 mm
Road/shell height	0.2 mm	0.2 mm
Road/shell print speed	40 mm/s	40 mm/s
In-fill	Printed grid, 100 % lines printed at print speed of 40 mm/s	Injected, 100 % by volume injected at flow rate of 12.5 mL/second
Print time	2940 s	800 s
Charpy impact strengths ± sd	12.93 ± 0.79 kJ/m^2	13.40 ± 0.56 kJ/m^2

Table 1 provides the process settings for five tested impact specimens made by the reference (material extrusion) and injection printing methods. As indicated in Table 1, the nominal temperatures and print speeds for both parts were the same, as were the specimens' length, width, and height dimensions. However, the replacement of the printed lines with injected cavities provides significant improvements in production time and part properties. Table 1 indicates that a constant print speed of 40 mm/s was used in material extrusion for printing the walls and internal line-patterned fill. The same print speed was used for printing the shell walls by the injection printing method for comparison purposes with material injected into the internal cavities at a flow rate of 12.5 mL/s. This part was produced as shown in the left cross-section of Fig. 3, with a checkerboard pattern of four layers height offset by two layers as previously discussed with respect to Fig. 2. The print time for the reference process is 2940s, 3.7 times longer than the 800 s required for injection printing. The parts were subsequently V notched for a Charpy impact test; the last row of the table provides the Charpy impact strengths that are subsequently discussed with images of the fracture

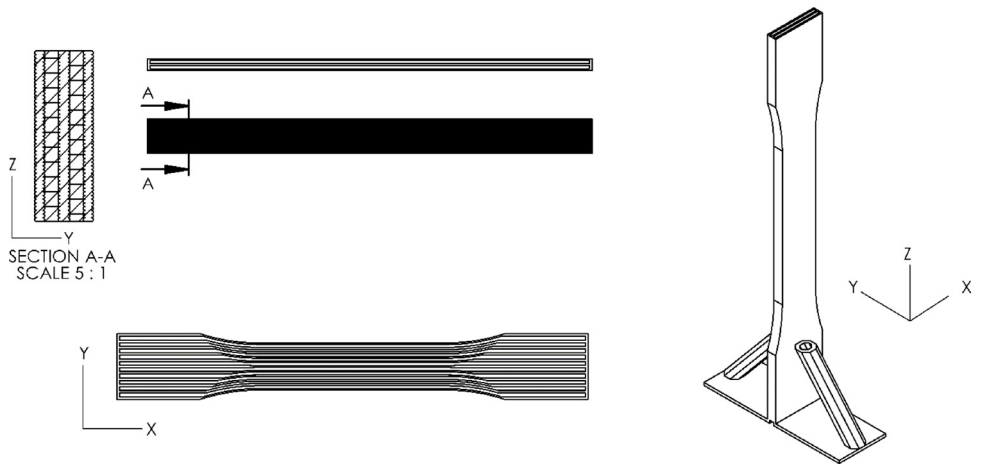

Fig. 3. Samples printed for this work including (top left) impact specimen made with alternating cavities, (bottom left) horizontal specimen made with varying shell and cavity widths, and (right) vertical tensile specimen made with alternating injections.

Table 2
Production and performance statistics for in-plane printed tensile specimens.

	Material Extrusion	Injection Printing
Build plate temperature	100 °C	100 °C
Nozzle temperature	230 °C	230 °C
Road/shell width	0.5 mm	0.5 − 0.62 mm
Road/shell height	0.2 mm	0.3, then 0.19 mm
Road/shell print speed	40 mm/second	40 mm/second
In-fill	Printed grid, 100 % by volume printed as grid at speed of 40 mm/second	Injected, 100 % by volume injected at flow rate of 14.7 mL/second
Print time, per part	2700 s	880 s
Elastic modulus, mean ± sd	1630 ± 95 MPa	1974 ± 133 MPa
Ultimate stress, mean ± sd	28.79 ± 1.56 MPa	42.50 ± 0.48 MPa
Strain to failure, mean ± sd	2.69 ± 0.32 %	3.64 ± 0.49 %
Energy to failure, mean ± sd	0.448 ± 0.092 MJ/m^3	0.914 ± 0.166 MJ/m^3

surface in the results section.

For production of the horizontal tensile specimen shown at middle of Fig. 3, the shell printing and subsequent cavity injections used varying road and cavity widths along the length of the part. This part was produced with 11 shell walls that define 10 cavities along its 127 mm length. At the middle of the part where the width is 12.7 mm, the shell walls are 0.5 mm wide while the intervening cavities are slightly wider, around 0.72 mm. At the ends of the part where the width is 17.7 mm, the shell walls are 0.62 mm wide while the intervening cavities are 1.09 mm. By varying the width of the shell walls and cavity, the part can be produced without adding extra walls and cavities at the ends of the part that would otherwise be required if the roads and cavities were constant width. As such, the part can be more quickly produced with improved part properties. The injection printed part was produced using five layers of stacked cavities, each cavity being defined by shell walls formed with three layers of roads. The bottom layer had a road height of 0.3 mm above which were 15 roads deposited with a height of approximately 0.19 mm to comprise the nominal part thickness of 3.18 mm. Accordingly, the first cavity had a nominal depth of 0.68 mm with the four cavities above each had nominal depths of 0.57 mm. Table 2 provides the production and performance statistics for the horizontal tensile specimens produced by the material extrusion and injection printing processes. It is observed that significant increases in speed (a factor of 3.07) were achieved along with significant improvements in part properties as will be described in more detail in the results section.

The strength in the vertical direction is also of interest. Accordingly, the vertical test specimen was produced with three shells and two cavities spanning the 3.2 mm thickness in the same manner described for the impact specimen and Fig. 2. The primary difference is that the roads comprising the outer shells of the injection printed parts were provided with alternating widths to provide undercutting layers as indicated in the left shell wall of Fig. 2. The use of the varying shell wall thicknesses allows for greater volumetric printing of the shell wall while also increasing the contact area between the injected volume and the previously printed shells. Given the small cross-sectional area of the vertically printed tensile bar depicted at right in Fig. 3, it was found necessary to reduce the print velocity during conventional 3D printing to avoid the part melting down during production. Accordingly, the nominal print speeds were set to 10 mm/s as indicated in Table 3. For injection printing, the flow rate for injection of material into each of the cavities was set to 2.5 mL/s. These settings were found to reliably produce the vertical tensile specimen, but the print time per specimen was 16,500 s for the reference process and 5700 s for injection printing. The injection printed parts were very glossy, and exhibited slight creep, a rougher surface, and slightly increased thickness (5%) compared to the more slowly printed material extrusion specimens. It is observed that the injection printing method was 2.9 times faster than the reference process. In theory, traditional material extrusion could achieve a similar production rate simply by increasing the print velocity from 10 to 29 mm/s. However, this is not the case as the printing at this speed consistently resulted in excess creep and distortion such that the printed parts had the appearance of twisted ropes. The structural behavior of the vertical tensile specimens will be discussed in the results section.

4. Results

The impact energy statistics from testing of five notched specimens produced for each process are provided in the bottom row of Table 1. Individual observations for all specimens are provided in Appendix A; no outlying behavior was observed and no results from any test specimens were discarded. It was observed that the average Charpy impact energy for the injection printed impact specimens were slightly improved (3.6 %) relative to the specimens produced by the material extrusion process. Statistical analysis of the raw data according to a one-sided t-distribution for two samples of unequal variance indicates that there is a 14 % probability that the two additive manufacturing methods are equal with respect to Charpy impact energy absorption, suggesting that it is more likely than not that the injection printed specimens had improved properties. The consistency was improved by injection printing as indicated by its reduced standard deviation, but both processes are much lower than the 28.9 kJ/m^2 median reported for impact grade (n = 61, [19]) as well as the 16.4 kJ/m^2 median reported for unreinforced, flame retardant grades of ABS (n = 24, [20]). It is believed that the presence of random voids can be doubly damaging, not only in reducing the load-bearing volume of material to absorb impact but also in inducing stress concentrations internal to the part; Coasey et al. [21] discuss pertaining to nonisothermal welding in material extrusion and suggest that voids, in the correct size range and distribution, can enhance strength though crack reflection or arrest.

Fig. 4 provides the failure surfaces of impact specimens made by reference material extrusion (left) and injection printing (right). The images clearly show a greatly reduced void fraction in the injection printed parts. Image analysis was conducted in Matlab with grayscale conversion of the sections to black and white such that the sum of the black pixels is representative of the void fraction as shown in the detailed views. The void fraction for the reference material extrusion process is 7.13 % compared to 0.98 % for the injection printed specimen. These void fractions are generally consistent with the changes in the impact energies observed in Table 1.

The stress-strain behaviors for all in-plane tensile specimens are plotted in Fig. 5. The injection printed parts consistently demonstrate higher strength as well as greater strain to failure. For reference, a typical grade of ABS (Sabic Cycolac GPM5600) has an ultimate strength of 48 MPa. As shown in Table 2, the ultimate strengths are 28.8 MPa for material extrusion and 42.5 MPa for injection printing. The improved properties are believed due to the greater density achieved with the injection printing method as well as improved diffusion and healing due to the added heat provided by the greater volume of hot material injected into the cavities with the injection printing method. Appendix A provides the individual sample observations as well as the statistical analysis of the strain to failure, ultimate strength, and strain energy. All

Table 3
Production and performance statistics for vertically printed tensile specimens.

	Material Extrusion	Injection Printing
Build plate temperature	100 °C	100 °C
Nozzle temperature	230 °C	230 °C
Road/shell width	0.5 mm	0.5 and 0.7 mm
Road/shell height	0.2 mm	0.2 mm
Road/shell print speed	10 mm/s	10 mm/s
In-fill	Printed grid, 100 % by volume printed as grid at speed of 10 mm/second	Injected, 100 % by volume injected at flow rate of 2.5 mL/s
Print time, per part	16,500 s	5700 s
Elastic modulus, mean ± sd	1761 ± 38 MPa	1762 ± 141 MPa
Ultimate stress, mean ± sd	24.68 ± 0.88 MPa	27.3 ± 0.91 MPa
Strain to failure, mean ± sd	1.76 ± 0.09 %	2.35 ± 0.11 %
Energy to failure, mean ± sd	0.210 ± 0.020 MJ/m^3	0.375 ± 0.028 MJ/m^3

results indicate the injection printing outperforms material extrusion with respect to all these structural behaviors to more than the 99 % confidence level.

During tensile testing, crazing and whitening of the specimens was observed at multiple points along the length of the injection printed specimens whereas the specimens produced by material extrusion failed in a sudden, more brittle manner. An oblique view of the specimens is shown in Fig. 6, with annotations to some of the observed crazing and material whitening. Inspection of the fracture surfaces also reveals that the injection printed specimens had large, stepped fracture surfaces, transitioning across the shell walls and cavities that allow the injection printed parts to approach the strength of the molded parts. The fracture surface also shows the pull-out of a molded cavity portion. It is interesting to reflect on the fact that this fracture surface represents the weakest section of the injection printed part, and the presence of crazing at other locations provides strong evidence of the high fill fraction and consistency of the material morphology afforded by the process.

Fig. 7 plots the stress-strain behavior for all the vertical tensile specimens; no outlying behavior was observed or discarded. The ultimate strength, elongation to failure, apparent modulus, and strain energy are summarized in Table 3. Overall, the gains in the vertical tensile specimen are not as impressive as those observed in the horizontal, in-plane, tensile bars. The primary improvement with injection printing is the 33 % increase in strain to failure and 78 % increase in strain energy relative to material extrusion. While the t-tests suggest that the injection printing is statistically better than material extrusion with respect to strain to failure and ultimate strength and strain energy, the apparent modulus is essentially unchanged.

The vertical tensile specimens and their failure surfaces are shown in Fig. 8 and suggest the reason for the relatively poor part properties. Both sets of test specimens produced by material extrusion and

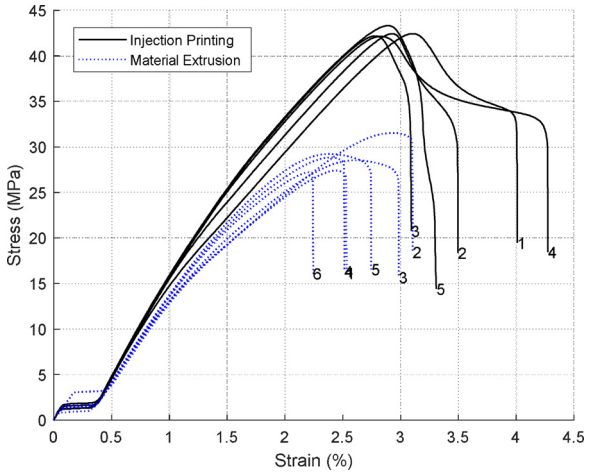

Fig. 5. Stress-strain diagrams for in-plane tensile specimens made by traditional material extrusion (dashed traces) and injection printing (solid traces).

injection printing had significant void fractions at the failure location. For the specimens produced by material extrusion, the parts included internal voids not only associated with the infill but also with the bonding between adjacent roads in the same printing layer. Meanwhile, the specimens made by injection printing had voids within the printed road that provides the shell, as well as between the shell wall and the material injected into the cavity. Observation of the voids in the shells of the injection printed section also suggest that the melt temperatures are too high such that there is excessive volumetric shrinkage. Observation of this injection printed section suggests that the alternating thick and thin roads in the outer shell (corresponding to the undercut

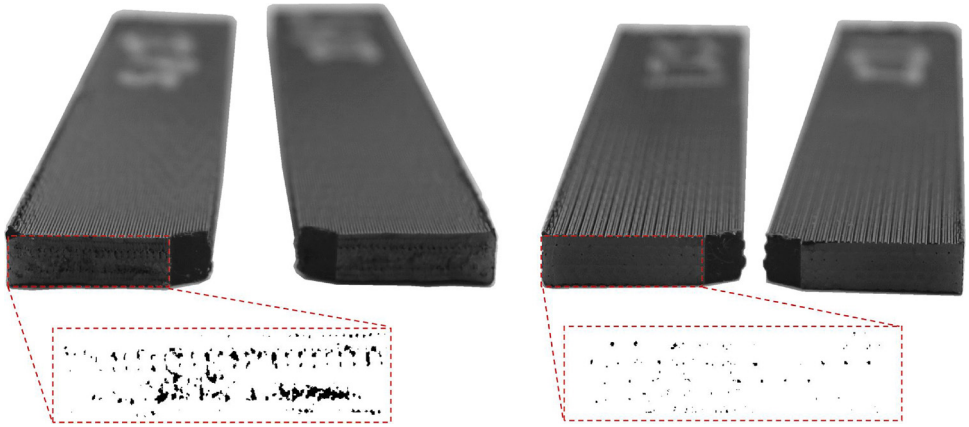

Fig. 4. Failure surfaces of impact specimens made by reference material extrusion (left) and injection printing (right) with detailed sections indicating the presence of voids in black.

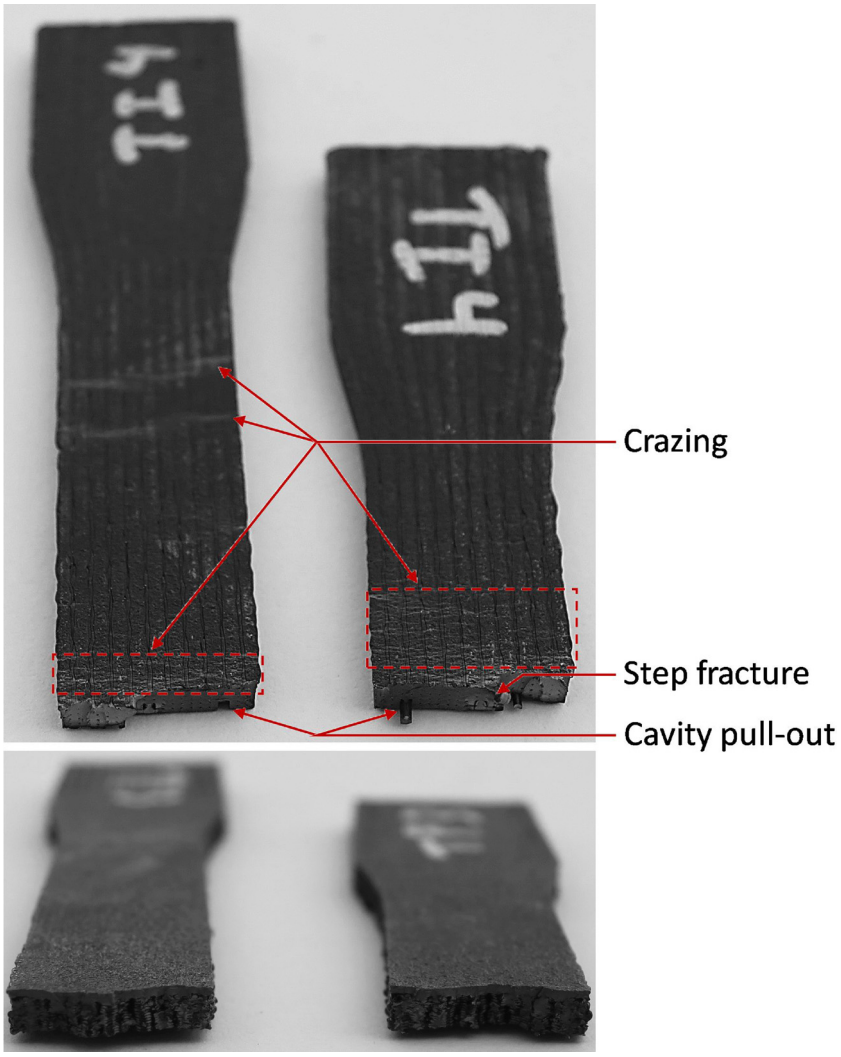

Fig. 6. Failure surfaces of in-plane tensile specimens made by traditional material extrusion (bottom) and injection printing (top).

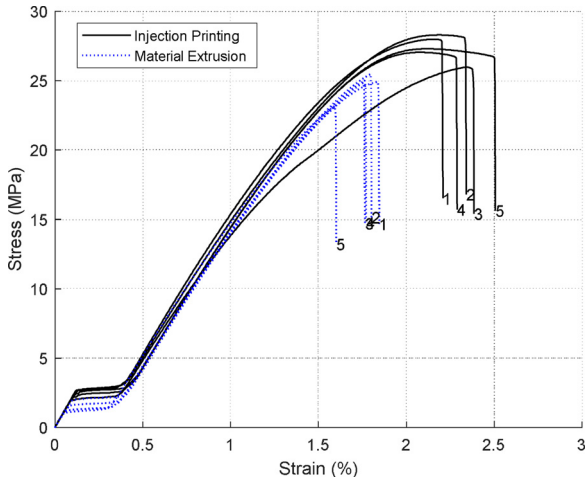

Fig. 7. Stress-strain diagrams for vertical tensile specimens made by traditional material extrusion (dashed traces) and injection printing (solid traces).

geometry described with respect to the left shell wall of Fig. 2) may be a bit too clever, since it may actually preclude complete cavity filling without improved melt pressure control (e.g. with a wider nozzle surface). The fact that the right indicated portion of the injection printed section is highly dense suggests that complete filling is possible albeit with local constraint of the melt filling by the ends of the cavity and the bottom surface of the nozzle as it traverses from right to left. As such, it is likely that fully dense parts can be achieved even for this challenging geometry with improvements as next discussed.

5. Discussion

All the validation with the reference material extrusion and injection printing processes were performed with a conventional nozzle design, i.e. an orifice diameter of 0.4 mm and an adjoining outer surface diameter of 0.9 mm. Such a small nozzle limits the width of the cavity that can be filled in a single pass, though tapered cavity widths leading to a smaller upper cavity width can be made by using printing with progressively thicker shell walls (e.g. 0.5 mm, 0.6 mm, 0.7 mm, and then 0.8 mm). Still, the printing of the shell walls is a relatively slow process compared to the injection of the material into the cavity. Accordingly, the use of current standard nozzles often makes it necessary to decompose relatively parts thicker than 2 mm (or more than about 3 times the outer surface diameter) into multiple cavities using one, or more, internal shell walls as previously described for the validation geometries. The need for printing of the internal shell walls is generally undesirable since (i) it is slow compared to injection printing of the same volume, and (ii) introduces potential failure modes associated with printing, injection, and end-use. To further improve the injection printing production speeds and part properties, it is

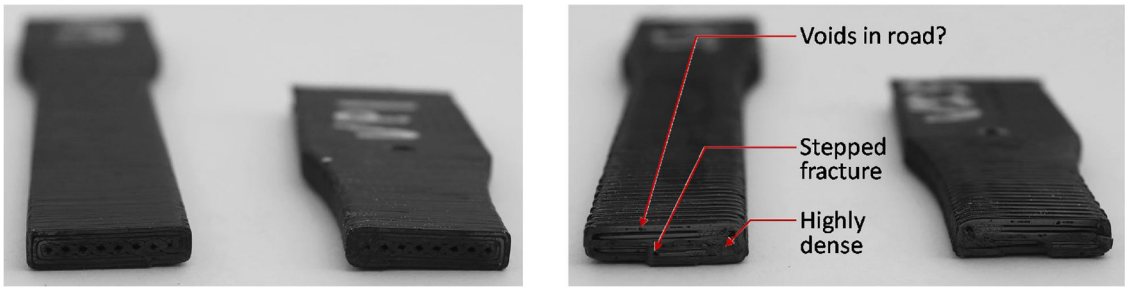

Fig. 8. Failure surfaces of vertical tensile specimens made by traditional material extrusion (left) and injection printing (right).

straightforward to use nozzles with larger lateral surfaces adjacent the nozzle orifice. Typical molded part thicknesses are around 3 mm, and the ASTM/ISO test standards often use similar thicknesses to ensure usefulness in application [22]. Similarly, increasing the nozzle surface diameter from 0.9 mm to 3 mm would allow the injection printing of part thicknesses up to 4 mm in a single pass without the need for internal shell walls and the use of two or more adjacent cavities. In theory, with no other changes to the described injection printing process, the print speeds for the impact and horizontal tensile specimens could increase from a factor of 3 to a factor of 5 compared to traditional material extrusion.

In validation, the heating capacity of the hot end was found to be a significant limiting constraint. With the standard nozzle and hot end, the Qidi XPro was found to only achieve a melting rate of 12.5 mL/s for the described ABS and processing conditions. This melting rate comports with a recently developed hot end (E3D Hemera) for which a maximum melting rate of 10 mL/s is specified. To improve the melting rate with traditional hot end designs, a longer melting section can be used wherein the first order approximation suggests that the melting rate is proportional to the square root of the nozzle length. Alternatively, the injection printing can make effective use of Go and Hart's "FastFFF" process [15] with its nut-feed extruder, laser-heated polymer liquefier, and resulting extrusion rate of 78 mL/s to quickly fill the printed cavities.

Currently, traditional material extrusion additive manufacturing is open loop with respect to the volume of the deposited roads. The assumption is that the volume of the input filament is known, the material is incompressible, and there is no slip in the infeed. All of these assumptions introduce inaccuracies that translate into variations in the printed products. A potential benefit of injection printing is the use of a filling stage with pressure monitoring such as with the instrumented hot end shown in Fig. 9. Fig. 9 also shows the instrumentation design for measuring the melt temperature and pressure in the hot end as motivated by prior use of the instrumented nozzle described by Coogan and Kazmer [9]. By moving the instrumentation from the nozzle into the hot end, the design allows the use of different sized nozzles to support reuse and diversity in application. By comparison with the prior instrumented nozzle, the design of Fig. 9 is greatly hardened, switching from a cantilever beam load cell supported by a single outrigger to a button-style load cell supported by a very stiff support plate, which is more rigidly positioned and supported with two shoulder bolts. The load pin is fully retained and can include a soldered or welded thermocouple for measuring melt temperature of the processed material.

The goal of using the instrumented hot end is to improve observability and controllability with control techniques akin to injection molding [23]. Specifically, injection molding uses a packing stage to admit additional material into the mold cavity to compensate for volumetric shrinkage as the processed material cools. In injection printing, the shell walls can be printed per conventional material extrusion using position control of the filament; monitoring the pressure provides feedback as to the filament consistency with respect to size and material properties. Then, in cavity filling, the instrumented hot end enables operation in a closed loop pressure control mode whereby the molten material completely fills the cavity; monitoring the amount of injected material provides feedback as to the consistency of the deposited road geometry forming the shells. Such hybrid use of position and pressure control ensures fully dense printed parts even better than the injection printed impact and tensile specimens depicted in Figs. 4 and 6. Such pressure based control was not used herein, but is a very promising research thrust to achieve part properties that directly rival

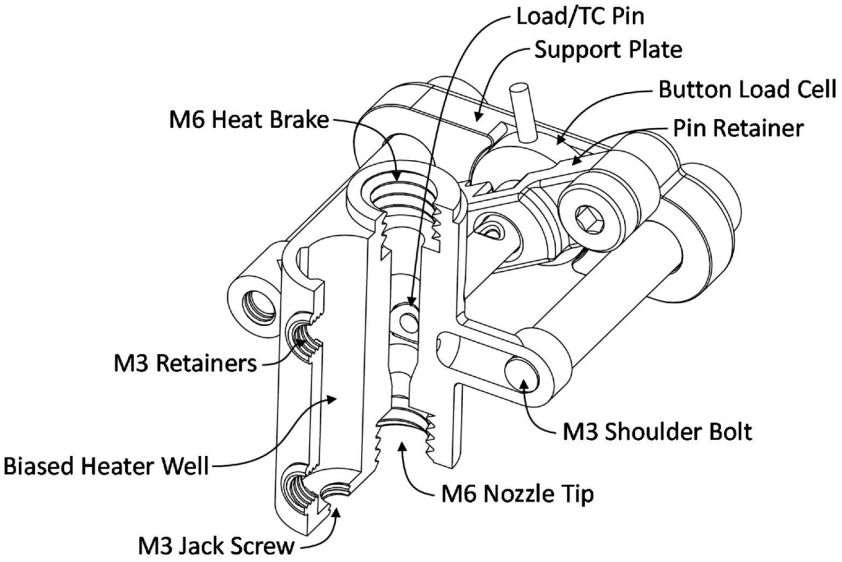

Fig. 9. Instrumented hot end with lofted slit channel.

injection molding.

6. Conclusion

Material extrusion is among the most accessible of additive manufacturing processes, with significant gains in the past decade enabled by widespread availability of machine components and open source code. However, further growth in material extrusion may be eclipsed by the growth of polyjet, powder bed, and CLIP processes in view of their greater production rates. The described injection printing process is a relatively simple hybrid of material extrusion and injection molding. While it doesn't fundamentally reduce the dimensionality of the printing process, it addresses the curse of dimensionality by greatly increasing the volume printed per interior cavity. The provided validation cases consistently demonstrated increases in production rates of more than 3 compared to traditional material extrusion while also improving part properties.

The validation cases also indicated two dominating constraints in the injection printing process using stock printers: (i) nozzle surface diameter and (ii) limited melting rates. The use of wider nozzle surfaces will clearly allow the filling of wider cavities with fewer internal shell walls. A second potential, but as yet unvalidated benefit, is the longer compaction time for the injected material by the residual pressure sustained by the trailing edge of the nozzle. Longer compaction times will compensate for volumetric shrinkage during cooling, resulting in stronger and more dimensionally stable parts akin to injection compression molding as for optical media [24]. Melting rate is also a significant constraint that also needs to be addressed in material extrusion to achieve higher production speeds. While these constraints are limiting, the injection printing method is already shown to have significant benefits with even greater gains possible with improved pre-processing algorithms, machine designs, and multi-material applications.

CRediT authorship contribution statement

David O. Kazmer: Conceptualization, Data curation, Formal analysis, Funding acquisition, Investigation, Methodology, Project administration, Resources, Software, Supervision, Validation, Visualization, Writing - original draft. **Austin Colon:** Investigation, Validation, Writing - review & editing.

Declaration of Competing Interest

The authors declare that they have no known competing financial interests or personal relationships that could have appeared to influence the work reported in this paper.

Acknowledgements

Portions of this work is based upon work supported by the National Science Foundation under Grant No. CNS #1644707 and # 1914651. Any opinions, findings, and conclusions or recommendations expressed in this material are those of the author(s) and do not necessarily reflect the views of the National Science Foundation.

Appendix A. Detailed Results

Specimen Type	Number	Process	Impact Energy (kJ/m^2)
Impact	1	Material Extrusion	11.67
Impact	2	Material Extrusion	12.42
Impact	3	Material Extrusion	13.72
Impact	4	Material Extrusion	13.71
Impact	5	Material Extrusion	13.02
Impact	6	Material Extrusion	13.06
		Mean:	12.93
		Standard Deviation:	0.786
Impact	1	Injection Printing	13.74
Impact	2	Injection Printing	13.07
Impact	3	Injection Printing	12.56
Impact	4	Injection Printing	13.82
Impact	5	Injection Printing	13.80
		Mean:	13.40
		Standard Deviation:	0.561
		Mean Difference, % (IP-ME)/ME:	3.61 %
		p(Injection Printing = Material Extrusion, n = 11)	14.12 %

Specimen Type	Number	Process	Strain to Failure (%)	Ultimate Strength (MPa)	Elastic Modulus (MPa)	Strain Energy (MJ/m^3)
Tensile	1	Material Extrusion	2.533	27.41	1521	0.385
Tensile	2	Material Extrusion	3.105	31.54	1540	0.571
Tensile	3	Material Extrusion	2.986	28.53	1586	0.521
Tensile	4	Material Extrusion	2.515	28.84	1711	0.408
Tensile	5	Material Extrusion	2.747	29.22	1753	0.482
Tensile	6	Material Extrusion	2.245	27.21	1667	0.324
		Mean:	2.688	28.79	1630	0.448
		Standard Deviation:	0.322	1.563	94.88	0.092
Tensile	1	Injection Printing	4.010	42.44	1764	1.022
Tensile	2	Injection Printing	3.497	42.43	1917	0.857
Tensile	3	Injection Printing	3.093	42.18	2048	0.733
Tensile	4	Injection Printing	4.275	42.13	2058	1.144
Tensile	5	Injection Printing	3.310	43.31	2082	0.813
		Mean:	3.637	42.50	1974	0.914
		Standard Deviation:	0.492	0.476	133.40	0.166

		Mean Difference, % (IP-ME)/ME:	35.3 %	47.6 %	21.1 %	103.9 %
		p(Injection Printing = Material Extrusion, n = 11)	0.42 %	0.00004 %	0.091 %	0.070 %
Vertical	1	Material Extrusion	1.846	24.92	1753	0.229
Vertical	2	Material Extrusion	1.803	25.48	1801	0.221
Vertical	3	Material Extrusion	1.764	24.82	1782	0.210
Vertical	4	Material Extrusion	1.772	25.02	1768	0.212
Vertical	5	Material Extrusion	1.602	23.17	1701	0.177
		Mean:	1.757	24.68	1761	0.210
		Standard Deviation:	0.093	0.881	38.22	0.020
Vertical	1	Injection Printing	2.208	27.99	1812	0.353
Vertical	2	Injection Printing	2.342	28.30	1797	0.386
Vertical	3	Injection Printing	2.386	25.97	1512	0.356
Vertical	4	Injection Printing	2.289	27.05	1843	0.359
Vertical	5	Injection Printing	2.508	27.30	1848	0.419
		Mean:	2.347	27.32	1762	0.375
		Standard Deviation:	0.112	0.908	141.42	0.028
		Mean Difference, % (IP-ME)/ME:	33.5 %	10.7 %	0.1 %	78.4 %
		p(Injection Printing = Material Extrusion, n = 10), %:	0.0011 %	0.081 %	49.3 %	0.0006 %

References

[1] B.N. Turner, S.A. Gold, A review of melt extrusion additive manufacturing processes: II. Materials, dimensional accuracy, and surface roughness, Rapid Prototyp. J. 21 (3) (2015) 250–261.

[2] R. Bellman, R.E. Kalaba, 7. Polynomial approximation, Dynamic Programming and Modern Control Theory, Academic Press, New York, 1965, p. 63.

[3] I.Q. Vu, L.B. Bass, C.B. Williams, D.A. Dillard, Characterizing the effect of print orientation on interface integrity of multi-material jetting additive manufacturing, J. Additive Manuf. 22 (2018) 447–461.

[4] R.J. Williams, et al., In situ thermography for laser powder bed fusion: effects of layer temperature on porosity, microstructure and mechanical properties, J. Additive Manuf. 30 (2019) 100880.

[5] D.J. McGregor, S. Tawfick, W.P. King, Mechanical properties of hexagonal lattice structures fabricated using continuous liquid interface production additive manufacturing, J. Additive Manuf. 25 (2019) 10–18.

[6] J.T. Belter, A.M. Dollar, Strengthening of 3D printed fused deposition manufactured parts using the fill compositing technique, PLoS One 10 (4) (2015) p. e0122915.

[7] C. Duty, J. Failla, S. Kim, T. Smith, J. Lindahl, V. Kunc, Z-Pinning approach for 3D printing mechanically isotropic materials, J. Additive Manuf. 27 (2019) 175–184.

[8] T.A. Osswald, J. Puentes, J. Kattinger, Fused filament fabrication melting model, J. Additive Manuf. 22 (2018) 51–59.

[9] T.J. Coogan, D.O. Kazmer, In-line rheological monitoring of fused deposition modeling, J. Rheol. 63 (1) (2019) 141–155.

[10] J. Go, S.N. Schiffres, A.G. Stevens, A.J. Hart, Rate limits of additive manufacturing by fused filament fabrication and guidelines for high-throughput system design, J. Additive Manuf. 16 (2017) 1–11.

[11] D.D. Phan, J.S. Horner, Z.R. Swain, A.N. Beris, M.E. Mackay, Computational fluid dynamics simulation of the melting process in the fused filament fabrication additive manufacturing technique, J. Additive Manuf. 33 (2020) 101161.

[12] M.P. Serdeczny, R. Comminal, D.B. Pedersen, J. Spangenberg, Experimental and analytical study of the polymer melt flow through the hot-end in material extrusion additive manufacturing, J. Additive Manuf. 32 (2020) 100997.

[13] V. Kishore, et al., Infrared preheating to improve interlayer strength of big area additive manufacturing (BAAM) components, J. Additive Manuf. 14 (2017) 7–12.

[14] A. Moshe, D. Kazmer, S. Johnston, R. Malloy, S. Kenig, Analysis of Variance in Capillary Rheometry, Polym. Eng. Sci. 56 (8) (2016) 895–904.

[15] J. Go, A.J. Hart, Fast desktop-scale extrusion additive manufacturing, J. Additive Manuf. 18 (2017) 276–284.

[16] T.J. Coogan, D.O. Kazmer, Modeling of interlayer contact and contact pressure during fused filament fabrication, J. Rheol. 63 (4) (2019) 655–672.

[17] D. Kazmer, Injection Mold Design Engineering, 2nd ed., Carl Hanser Verlag, Munich, 2016, p. 410.

[18] F. Kreith, W.Z. Black, Transient heat conduction, Basic Heat Transfer, Harper & Row, 1980, pp. 136–189.

[19] Overview of Materials for Acrylonitrile Butadiene Styrene (ABS), Impact Grade, Molded, (2019) Accessed on: December 13 http://matweb.com/.

[20] Overview of Materials for Acrylonitrile Butadiene Styrene (ABS), Flame Retardant Grade, Molded, (2019) Accessed on: December 13 http://matweb.com/.

[21] K. Coasey, K.R. Hart, E. Wetzel, D. Edwards, M.E. Mackay, Nonisothermal Welding in Fused Filament Fabrication, J. Additive Manuf. (2020) 101140.

[22] C.M. Eastman, N. Fereshetian, Information models for use in product design: a comparison, Comput.-Aided Des. 26 (7) (1994) 551–572.

[23] D. Kazmer, P. Barkan, Multi-cavity pressure control in the filling and packing stages of the injection molding process, Polym. Eng. Sci. 37 (11) (1997) 1865–1879.

[24] B. Fan, D.O. Kazmer, W.C. Bushko, R.P. Theriault, A.J. Poslinski, Simulation of injection-compression molding for optical media, Polym. Eng. Sci. 43 (3) (2003) 596–606.